Struct Multidisc Optim (2014) 49:643–655
DOI 10.1007/s00158-013-1000-z

RESEARCH PAPER

Design of actively-cooled microvascular materials: a genetic algorithm inspired network optimization

Soheil Soghrati · Alejandro M. Aragón · Philippe H. Geubelle

Received: 2 November 2012 / Revised: 7 August 2013 / Accepted: 14 September 2013 / Published online: 5 October 2013

Abstract The design of a microvascular flow network embedded in an actively-cooled polymeric material is presented. A multi-objective Genetic Algorithm (GA) combined with the finite element method is first used to determine the quasi-optimized network configurations and provide insight into the behavior of the actively-cooled material. The objective functions and constraints involve improving the flow efficiency and minimizing the void volume fraction of the material, while maintaining an allowable temperature in the system. A periodic configuration is adopted for the embedded network based on the results of this study. We then solve an optimization problem at a considerably lower computational cost to improve the optimized network configuration. To determine the final design, we implement the information obtained from the GA optimization to describe the geometry of the embedded network in a simple mathematical form and conduct a parameter study to evaluate its optimized shape.

S. Soghrati (✉)
Mechanical and Aerospace Engineering Department,
The Ohio State University,
201 West 19th Avenue, Columbus, OH, USA
e-mail: soghrati.1@osu.edu

A. M. Aragón
School of Architecture, Civil and Environmental Engineering,
École polytechnique fédérale de Lausanne,
1015 Lausanne, Switzerland

P. H. Geubelle
Aerospace Engineering Department,
University of Illinois at Urbana-Champaign,
104 South Wright Street, Urbana, IL, USA

Keywords Genetic algorithms · Optimization · Active cooling · Convective heat transfer · Microvascular materials · Finite element method

1 Introduction

Bio-mimetic materials with embedded microvascular networks have been considered for a variety of autonomic applications, including self-healing and active-cooling (Toohey et al. 2007; Olugebefola et al. 2010). In self-healing microvascular systems, microchannels are filled with an uncured healing agent, which is released when cracks intersect with the channels to restore the material stiffness and strength (Toohey et al. 2007; Hansen et al. 2009). In active cooling, the continuous flow of a coolant in the microchannels is employed to reduce the temperature of the system (Pastukhov et al. 2003; Kozola et al. 2010). In most microvascular materials such as microelectromechanical systems (MEMS) (Wang et al. 2005; Wei et al. 2007; Oueslati et al. 2008), active cooling is merely achieved by convecting the heat out of the system through the flow in the microchannels. The microvascular network embedded in these materials acts as a heat sink, as the coolant absorbs the heat from the adjacent solid and removes it from the system. In larger domains, however, the amount of the heat removed through convection may correspond to a small portion of the thermal energy given to the system. Thus, an efficient active cooling relies mostly on the configuration of the embedded network to effectively redistribute the heat inside the material by convecting it from warm to cool regions (Shipton 2007). In this paper, we study the design of the embedded network in an actively-cooled microvascular polymeric plate belonging to the latter category.

Besides reducing the maximum temperature of the system, other factors might affect the optimal configuration of the embedded network in actively-cooled materials. For example, minimizing the adverse impact of the network on the mechanical properties of the material and quantifying the flow efficiency can be included in the design objectives. Moreover, constraints such as those imposed by the available manufacturing techniques must be incorporated during the design process. Such parameters are implemented as a set of objective and constraint functions to optimize the topology of the microvascular network (Evgrafov 2006; Aragón et al. 2008). The non-convex nature of the resulting optimization problem, i.e., the existence of multiple local optima, is one of the challenges in determining the optimal configuration of the network. Moreover, in some problems including the actively-cooled material system studied in this manuscript, the network configurations that are optimal for minimizing some objective functions do not yield satisfactory results for the others. Some researchers address this issue by casting all the objective functions into a single objective using a weighting method to resolve this problem (Park et al. 2004; Chen et al. 2010).

Varied optimization techniques are adopted in the literature for the design of flow network problems. Gradient based optimization methods, which are among the most efficient approaches in the structural topology optimization (Rozavany 2009), have also been applied to the design of flow network problems (Gersborg-Hansen et al. 2005). A set of discrete diameter variables is implemented in Klarbring et al. (2003) to determine the optimal topology and size of the flow network using a gradient-based technique. Another approach to obtain the optimal configuration of the network in such problems is based on the constructal theory (Bejan 1997; Bejan and Lorente 2008). In this method, the constructal law uses a series of optimization and organization steps that start from an elemental level and evolve towards the optimal network configuration. One of the methodologies that has successfully been applied to discrete optimization problems, such as those studied here, is the family of evolutionary algorithms. Among these methods, Genetic Algorithms (GA) have received the most attention (Goldberg 1989, 2002). GA applies biology-inspired genetic operators to evolve a set of candidate solutions towards better configurations for the problem at hand. Thus, regardless of the type of the problem being solved, GA searches the entire decision space for the optimized designs only based on the specified values of the objective functions and constraints. This flexibility of GA has extended its applicability to a wide variety of optimization problems including the design of flow networks and microvascular materials (Simpson et al. 1994; Prasad and Park 2004; Nible et al. 2006; Kumar et al. 2006; Aragón et al. 2008, 2011).

In this work, we employ GA to inspire the optimized configurations of the embedded network in a microvascular epoxy plate and provide insight on its optimized design. The objective functions include i) the maximum temperature of the plate, ii) the void volume fraction associated with the embedded network, and iii) the pressure drop needed to circulate the coolant in the microchannels. An important feature of these objective functions is their competing nature. For instance, networks with low void volume fractions often yield high values of the pressure drop, and those with low pressure drops cannot effectively contribute to cooling of the plate. In such problems, using Multi-Objective Evolutionary Algorithms (MOEAs) (Fonseca and Fleming 1993; Horn et al. 1994; Kukkonen and Lampinen 2005; Deb et al. 2002) yields better results compared to simple GA, where all objective functions are casted into a single one by assigning different weights. In this study, we employ the algorithm introduced by Deb et al. (2002), known as the Non-dominated Sorting Genetic Algorithm (NSGA-II), for evaluating the optimized topology of the network. The NSGA-II uses the concept of *Pareto optimality* to compute a set of optimized candidate solutions, among which one can select the final design according to desired values of each objective function. This feature of the NSGA-II has been one of the main motivations of employing that in this work, as it yields a pool of optimized candidate network configurations, among which the final design can be selected based on manufacturing constraints and other engineering considerations.

Using a GA-based approach to find the optimized shape of the networks has two main drawbacks: the high computational cost of simulations (Sigmund 2011) and the complex configuration of resulting optimized networks. Moreover, the network configuration in some materials such as those found in microvascular woven composites (Esser-Kahn et al. 2011; Soghrati et al. 2012a) is highly controlled by manufacturing constraints, allowing only specific network configurations. To address this issue, we propose a hierarchical synergistic design approach, in which we first adopt a periodic configuration for the microvascular network inspired by the results of the GA optimization over the entire component. At this step, we perform the analyses over several smaller subdomains to obtain less complex optimized configurations at a fraction of the original computational cost. The observations made at this step suggest that a parametric square wave function can best describe the optimized network configuration. We then perform a parametric shape optimization as the final design step to evaluate the optimized geometry of the embedded microchannels. Unlike the previous GA problems, this parametric shape optimization has a considerably lower computational cost and provides an easy way to incorporate the manufacturing constraints in the design process. The three-level synergistic

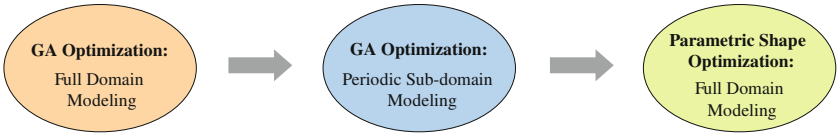

Fig. 1 Three-level design of the actively-cooled microvascular component, where the final optimized configurations are determined through a parametric study shape optimization according to the information obtained from the previous GA optimization studies

design process of the actively-cooled microvascular system adopted in this work is depicted in Fig. 1, where, from left to right, the search space is further confined according to the information obtained from previous steps to reach the final design.

The remainder of this paper is organized as follows: In the next section, we present the governing equations used to evaluate the thermal response of actively-cooled materials together with their finite element method (FEM) approximation. In Section 3, we describe the design problem of interest and discuss the associated objective functions and constraints involved in the optimization of the microvascular network. A brief description of the NSGA-II algorithm is presented in Section 4 and the implementation of this method for evaluating the optimized configuration of the embedded network is studied in Section 5. In Section 6, we adopt a periodic network configuration and use NSGA-II to determine the optimized configuration of the network over multiple subdomains of the original problem. The parametric shape optimization employed to obtain the final design of the network is described in Section 7.

2 Thermal response of actively-cooled microvascular materials

Figure 2 illustrates the schematic of a microvascular material, composed of an open domain $\Omega = \Omega_s \cup \Omega_f \subset \mathbb{R}^2$ with closure $\overline{\Omega}$, where Ω_s and Ω_f are the solid and the fluid phases, respectively. The boundary $\Gamma = \overline{\Omega} \backslash \Omega$ with outward unit normal $\mathbf{n}$ is divided into two mutually exclusive partitions Γ_T and Γ_q such that $\Gamma = \Gamma_T \cup \Gamma_q$ and $\Gamma_T \cap \Gamma_q = \emptyset$. Γ_T corresponds to regions where the Dirichlet boundary conditions with a temperature $\bar{T} : \Gamma_T \to \mathbb{R}$ are imposed. The Neumann boundary conditions with the applied heat flux $\bar{q} : \Gamma_q \to \mathbb{R}$ are prescribed at Γ_q. Assuming $f : \Omega \to \mathbb{R}$ as the applied heat source, the strong form of governing conjugate heat transfer equations is expressed as follows: Given the thermal conductivity $\boldsymbol{\kappa}_{s,f} =: \overline{\Omega} \to \mathbb{R}^2 \times \mathbb{R}^2$, fluid density $\rho_f : \Omega_f \to \mathbb{R}$, and fluid specific heat $c_p : \Omega_f \to \mathbb{R}$, find the temperature field $T : \overline{\Omega} \to \mathbb{R}$ such that

$$\begin{aligned} \nabla \cdot (\boldsymbol{\kappa}_s \nabla T) + f &= 0 \quad \text{in } \Omega_s, \\ \nabla \cdot \left(\boldsymbol{\kappa}_f \nabla T\right) - \rho_f c_p \mathbf{v}.\nabla T + f &= 0 \quad \text{in } \Omega_f, \\ T &= \bar{T} \quad \text{on } \Gamma_T, \\ \boldsymbol{\kappa}_s \nabla T \cdot \mathbf{n} &= \bar{q} \quad \text{on } \Gamma_q, \end{aligned} \tag{1}$$

with solid-fluid interface conditions

$$\begin{aligned} T_s &= T_f \quad \text{on } \overline{\Omega_s} \cap \overline{\Omega_f}, \\ \boldsymbol{\kappa}_s \nabla T_s \cdot \mathbf{n}_s + \boldsymbol{\kappa}_f \nabla T_f \cdot \mathbf{n}_f &= 0 \quad \text{on } \overline{\Omega_s} \cap \overline{\Omega_f}, \end{aligned}$$

where $\mathbf{n}_s$ and $\mathbf{n}_f$ are outward unit normals to the solid and fluid boundaries, respectively.

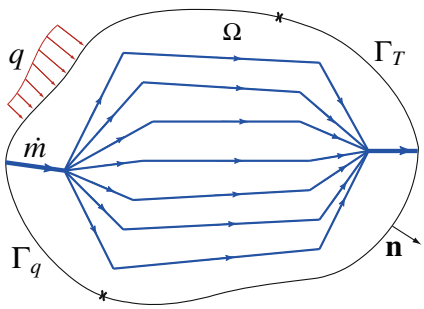

Fig. 2 Schematic of the 2D domain of an actively-cooled microvascular material with a mass flow rate $\dot{m}$ circulating in the microchannels. The boundary with outward unit normal $\mathbf{n}$ is divided into two regions Γ_T and Γ_q corresponding to the Dirichlet and Neumann boundary conditions, respectively

Due to the small diameters of the microchannels and the laminar nature of the flow, we will provide an alternative simplified boundary value problem to that presented by (1). Let the representation of the network be simplified as an ensemble of m lines, lower order manifolds of zero measure in $\mathbb{R}^2$. Each line γ_j thus represents the jth microchannel. Using the assumptions of fully developed velocity and temperature profiles in the network, the heat convection in each microchannel can be modeled through a simple energy balance (Kays et al. 2004). The convected heat energy is considered as a heat sink acting along the jth microchannel as $s_j = c_p \dot{m}_j dT/d\xi_j$ (Bronzino 2000), where $\dot{m}_j$ is the coolant mass flow rate and $dT/d\xi_j$ is the average fluid temperature gradient along the microchannel centerline direction. Due to the temperature continuity constraint along the fluid-solid interface, this temperature is equal to the adjacent solid temperature.

The network, now represented by $\Gamma_I = \cup_{j=1}^{m} \gamma_j$, divides the solid phase into n smaller subregions ω_i, such that $\overline{\cup_{i=1}^{n} \omega_i} = \Omega_s$ and $\cap_{i=1}^{n} \omega_i = \emptyset$. The boundary of each solid subdomain $\partial\omega_i \equiv \overline{\omega_i} \setminus \omega_i$ has outward unit normal $\boldsymbol{n}_i^s$. Dirichlet and Neumann boundaries from problem

(1) can still be used, as for example, $\Gamma_T \subset \{\cup_i \partial\omega_i\}$, and $\Gamma_T \cap \{\cup_i \partial\omega_i\} = \Gamma_T$. The alternative boundary value problem then seeks the solution of the temperature field in solid subdomains only: Given $\boldsymbol{\kappa}_s$, f_i[1], c_p, as before, find the temperature field $T_i : \overline{\omega}_i \to \mathbb{R}$, such that

$$\begin{aligned} \nabla \cdot (\boldsymbol{k}_s \nabla T_i) + f_i &= 0 && \text{on } \omega_i, \\ T_i &= \bar{T} && \text{on } \Gamma_T \cap \partial\omega_i, \\ \boldsymbol{k}_s \nabla T_i \cdot \boldsymbol{n}_i^s &= \bar{q} && \text{on } \Gamma_q \cap \partial\omega_i, \\ \boldsymbol{k}_s \nabla T_i \cdot \boldsymbol{n}_i^s &= -c_p \dot{m}_j \frac{dT_i}{d\xi_j} && \text{on } \left\{\cup_j \gamma_j\right\} \cap \partial\omega_i, \end{aligned} \quad (2)$$

where the effect of the fluid convection is taken into consideration via the last line of the above equation.

Defining a set of trial solutions $\mathcal{T}$ and the variational space $\mathcal{W}$ as

$$\mathcal{T} = \left\{T_i \in H^1(\omega_i) : T_i = T_j \text{ on } \partial\omega_i \cap \partial\omega_j \neq \emptyset,\ T_i\big|_{\Gamma_T} = \bar{T}\right\},$$
$$\mathcal{W} = \left\{v_i \in H^1(\omega_i) : v_i = v_j \text{ on } \partial\omega_i \cap \partial\omega_j \neq \emptyset,\ v_i\big|_{\Gamma_T} = 0\right\},$$

the weak form is expressed as: Find $T_i \in \mathcal{T}$ such that $\forall \omega_i$

$$a(v_i, T_i) + a(v_i, T_i)_{\Gamma_I} = (v_i, f_i) + (v, \bar{q})_{\Gamma_q} \quad \forall v_i \in \mathcal{W}, \quad (3)$$

where the linear and bilinear forms are given by

$$\begin{aligned} a(v_i, T_i) &= \int_{\omega_i} \nabla v_i \cdot (\boldsymbol{k}_s \nabla T_i)\ d\omega, \\ a(v_i, T_i)_{\Gamma_I} &= \sum_{j=1}^{m} \int_{\gamma_j} v_i c_p \dot{m}_j \frac{dT_i}{d\xi_j}\ d\partial\omega, \\ (v_i, f_i) &= \int_{\omega_i} v_i f_i\ d\omega, \\ (v_i, \bar{q})_{\Gamma_q} &= \int_{\Gamma_q} v_i \bar{q}\ d\partial\omega. \end{aligned}$$

To obtain a Galerkin FEM approximation for this problem, we first discretize each subdomain ω_i into M_i mutually exclusive finite elements, such that $\omega_i^h = \overline{\cup_{k=1}^{M_i} \omega_{ik}^h} = \omega_i$. The node sets corresponding to the elements of two contiguous subdomain boundaries are enforced to be equivalent to enforce the temperature continuity condition. In other words, a conforming mesh is required in the solid subdomain boundaries. A set of N Lagrangian shape functions ϕ are then employed to approximate $\mathcal{T}^h = \mathcal{W}^h \subset \mathcal{W}$ such that $\forall \boldsymbol{x} \in \omega_i^h$, $\mathcal{W}^h = \left\{w \in C^0\left(\omega_i^h\right) : w(\boldsymbol{x}) = \sum_{j=1}^{N} \phi_j(\boldsymbol{x}) T_j^h\right\}$, where T_j^h are the nodal temperature values. One could also implement mesh-independent generalized FEM to provide an accurate approximation for (3) using meshes that do not conform to the microchannels' geometry (Soghrati et al. 2012b; Soghrati and Geubelle 2012). It must be noted that before approximating the temperature field in this problem, we need to compute the values of the coolant mass flow rate $\dot{m}$ in each microchannel, as described in the next section.

[1] Understood as the restriction of the body force on the subdomain, i.e., $f_i \equiv f|_{\omega_i}$.

3 Problem description and design variables

The geometry and the boundary conditions of the 2D design problem studied in the following sections are illustrated in Fig. 3. The 50×5 cm^2 epoxy plate with the thermal conductivity $\kappa = 0.3$ W/m K is insulated along the left and the right sides. Other boundary conditions include the prescribed temperature $\bar{T} = 20\,^\circ$C and the constant heat flux $\bar{q} = 1680$ W/m along the bottom and the top edges, respectively. The value of the heat flux is selected such that the maximum temperature of the material in the absence of the flow is $T_{\max} = 300\,^\circ$C. Figure 3 also depicts the schematic of a possible configuration of the microvascular network used for active cooling of the epoxy plate, where all the microchannels have a diameter $D = 200\,\mu$m. We employ ethylene glycol as the coolant with an inlet temperature $T_{\text{in}} = 20\,^\circ$C and properties $c_p = 2.44$ kJ/kg K and $\rho_f = 1113.2$ kg/m^3.

The point lattice used to discretize the microvascular network is illustrated in the inset of Fig. 3, where the microchannels can be created in the horizontal or vertical directions between two adjacent nodes. The network template, i.e., a network with all possible microchannels for a given grid, can be mathematically expressed with a graph data structure $\mathbb{G} := (V, E)$ (Aragón et al. 2011). The edges $e_i \in E(\mathbb{G})$ and vertices $v_i \in V(\mathbb{G})$ of this graph represent the microchannels and their endpoints, respectively. A particular configuration of the network similar to that shown in Fig. 3 can be considered as a subgraph of $\mathbb{G}$, $\bar{\mathbb{G}} := \left(\bar{V}, \bar{E}\right)$, where $\bar{E} \subseteq E$ and $\bar{V} \subseteq V$. For the current problem, the template network is built on an $n_x \times n_y$ grid with equally-distanced vertices. The number of the edges in the corresponding template network is $|E(\mathbb{G})| = 2n_x n_y - n_x - n_y$. Using a set of k discrete microchannel diameters $\mathcal{D} := \{D_i\}_{i=1}^{k}$, we have a total number of $k^{|E(\mathbb{G})|}$ possible configurations for the embedded network. These include the case for which $D_i = 0$, i.e., the absence of a microchannel between two adjacent vertices. The optimization problem is then defined as finding the values of D_i for each microchannels to minimize a set of m objective functions $\Phi = \{\phi_i\}_{i=1}^{m}$, subject to the constraints $\Psi = \{\psi_i\}_{i=1}^{n}$. These objective functions and constraints are described next.

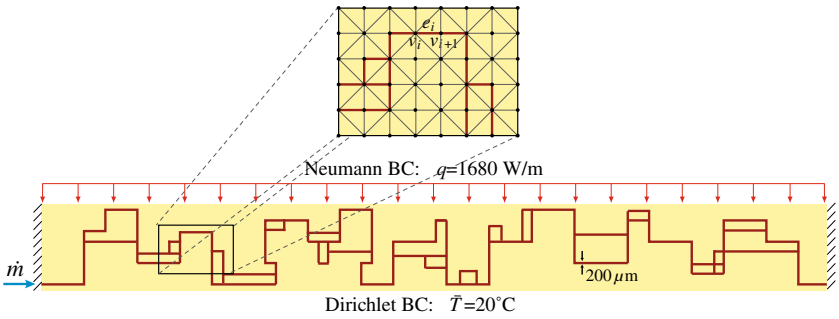

Fig. 3 Geometry, boundary conditions, and the schematic of the embedded microvascular network in the design problem with dimensions 50×5 cm^2. The inset illustrates the structured triangular finite element mesh and the background grid used for the discretization of domain and the flow network, respectively

Maximum temperature We define the first objective function as the maximum predicted temperature in the domain, i.e.,

$$\phi_1 \equiv T_{\max} := \sup T^h(\mathbf{x}), \forall \mathbf{x} \in \overline{\Omega}_s^h, \tag{4}$$

where T^h is obtained from the finite element approximation of (3).

Void volume fraction While reducing the maximum temperature of the domain, an appropriate configuration for the microvascular network must be minimally invasive with respect to the mechanical properties of the material. As a first-order approximation, the impact on the stiffness of the microvascular component can be linked to the volume fraction V_f associated with the embedded network defined as

$$\phi_2 \equiv V_f := \frac{\sum_{e_i \in E(\mathbb{G})} L_i D_i}{A_{\Omega^h}}, \tag{5}$$

where L_i is the length of microchannel i and A_{Ω^h} is the area of the domain.

Pressure drop and required power The third objective function is defined as the pressure drop between the inlet and the outlet, i.e.,

$$\phi_3 \equiv \Delta p := p_{v_{\text{in}}} - p_{v_{\text{out}}}, \tag{6}$$

where $p_{v_{\text{in}}}$ and $p_{v_{\text{out}}}$ are the values of the pressure at the inflow and outflow vertices, respectively. Assuming a fully-developed laminar flow in the microchannels, the pressure drop between the end-points of a microchannel is computed through the Hagen-Poiseuille law,

$$\Delta p_i = \frac{128 \mu \dot{m}_i L_i}{\rho \pi D_i^4}, \tag{7}$$

where μ is the dynamic viscosity of the fluid. For ethyline glycol, the coolant used in the test problem, a constant value of the dynamic viscosity $\mu = 3.9^{-4}$ kg/m s at $T = 70\,^{\circ}$C is used in the numerical simulations. This temperature is approximately equal to the average temperature of the circulating fluid in the networks studied in this work. Using the principle of the conservation of the mass at each vertex, the pressure drop associated with the coolant flow at each vertex is obtained by assembling (7) for the entire network and solving the resulting system of linear equations, $\mathbf{kp} = \dot{\mathbf{m}}$. In this equation, $\mathbf{k}$ is the characteristic matrix and $\mathbf{p}$ and $\dot{\mathbf{m}}$ are the vectors associated with the values of the pressure and the mass flow rate at each vertex, respectively. The flow boundary conditions incorporated in this linear system of equation include the prescribed values of the mass flow rate at the entrance vertex and the atmospheric pressure at the outlet. After evaluating the pressure drop at each vertex, one can use (7) to compute the coolant mass flow rate in each microchannel. Further details regarding the evaluation of the pressure values in discrete networks can be found in Brebbia and Ferrante (1983).

Minimizing the pressure drop as described by (6) and (7) minimizes the power P needed to circulate the coolant in the embedded network:

$$P = \frac{\dot{m} \Delta p}{\rho_f}. \tag{8}$$

If the available power for pumping the coolant is set fixed, the mass flow rate in (8) can be simply modified before evaluating the temperature field by scaling the flow rate in each microchannel to maintain a constant power. In the following sections, we use both the constant flow rate and the constant power strategies to design the microvascular networks and study how each assumption affects the resulting optimized configurations. It must be noted that for the constant power strategy, the pressure drop is still considered as one of the objective functions to facilitate pumping the coolant in the microchannels.

Connected networks constraint The key constraint on a subgraph of $\mathbb{G}$ to represent a feasible network for active cooling of the system is to provide a connected path between the inflow and outflow vertices. This constraint is necessary to discard disconnected networks created throughout the GA optimization, for which there is no solution to the flow problem. In graph theory, a *connected graph* is defined as a graph where every vertex is reachable from every other vertex. Thus, a feasible configuration for the microvascular network is represented by a connected subgraph,

$\bar{\mathbb{G}} := \left(\bar{V}, \bar{E}\right)$, provided that it includes both the inflow and outflow vertices as well. This can be mathematically quantified as

$$\psi_1 := \max\left(c\left(\bar{\mathbb{G}}\right) - 1, 1 - \deg\left(v_{\text{in}}\right), 1 - \deg\left(v_{\text{out}}\right)\right), \quad (9)$$

where $c\left(\bar{\mathbb{G}}\right)$ is the number of the connected components in subgraph $\bar{\mathbb{G}}$, and $\deg(v_{\text{in}})$ and $\deg(v_{\text{out}})$ are the degrees (number of the incident edges) at the inflow and the outflow vertices, respectively. The condition $\psi_1 = 0$ to satisfy the connectivity constraint is achieved if $c\left(\bar{\mathbb{G}}\right) = 1$, and there is at least one connected edge at both the inflow and outflow vertices.

Fluid temperature constraint We incorporate a constraint on the allowable temperature of the coolant to prevent it from exceeding the boiling point. We use $T_{f,\text{all}} = 190\,^{\circ}\text{C}$ as the maximum allowable temperature of the coolant, which is slightly lower than the boiling point of the ethylene glycol $T_{f,\text{boil}} = 197.3\,^{\circ}\text{C}$. The fluid temperature constraint is then incorporated by monitoring the temperature of the coolant at the vertices of the network and applying a penalty if it exceeds the allowable temperature.

An appropriate constraint function for the maximum coolant temperature must incorporate two features simultaneously: the number of the vertices where the allowable temperature is violated and the magnitude of the violation. The choice for this constraint has a crucial impact on the performance of the GA optimization as an inappropriate function can lead to *genetic drifts*, i.e., a premature convergence to non-optimal configurations. We adopt the following expression for this constraint

$$\psi_2 := \sum_{v_i \in V} \max\left(0, T_{f,v_i} - T_{f,\text{all}}\right)^{1/3}, \quad (10)$$

where T_{f,v_i} is the fluid temperature at vertex v_i. To better understand (10), assume a network for which the allowable temperature is exceeded by 1 °C at eight vertices compared to another network where this happens at only one vertex, but for 8 °C. The constraint function values obtained from (10) for these networks are $\psi_2^{(1)} = 8$ and $\psi_2^{(2)} = 2$, respectively, which denotes a higher chance of survival for the latter case. A lower penalty for networks where the allowable temperature is violated at fewer vertices leads to their higher chance to evolve into feasible configurations in the next generations of the GA optimization.

4 Multi-objective genetic algorithms

The NSGA-II optimization scheme can successfully handle the tradeoff between conflicting objective functions and constraints (Deb et al. 2002). This method employs the concept of *Pareto-optimality* to identify the population at each generation. Each individual in the population is encoded as a string (chromosome) $\mathcal{C}$ that represents a particular network configuration. Using the graph data structure introduced in Section 3, with $D = \{0, 200\}\ \mu$m, the adjacency matrix of the each graph is employed to encode the chromosomes. Hence, for chromosome $\mathcal{C} = \{1001011010...\}$, a unity value at the $i-$th position (allele) $\mathtt{A}_{\mathcal{C}}[i] = 1$ denotes the presence of a microchannel with $D = 200\,\mu$m at edge e_i, while $\mathtt{A}_{\mathcal{C}}[j] = 0$ means no microchannel is created at the $j-$th edge.

The optimization is initiated with a randomly generated population $\mathcal{P}_0$ of size $N_{\mathcal{P}}$. At each time t of the evolution process, we apply genetic operators *selection*, *cross-over* and *mutation* to $\mathcal{P}$ to obtain a new population $\mathcal{P}'$. This step uses tournament selection, uniform crossover, and a low probability of mutation, $p_m \leq 1/l_c$, where l_c is the length of the chromosome. To obtain the offspring population at $t+1$, the size is reduced back to $N_{\mathcal{P}}$ by using a Pareto-selection mechanism. During this selection process, the population is divided into mutually exclusive sets of feasible and unfeasible individuals, where an individual is considered feasible only if it satisfies all the constraint functions. A rank is then assigned to all individuals and those with the same rank form a front. The final population at the next generation is obtained by combining the front (or fronts) of lowest ranks. More details regarding the NSGA-II algorithm can be found in Deb et al. (2002).

5 GA optimization: full-domain simulations

In this first step of the optimization study, the NSGA-II is employed to determine the quasi-optimal configurations of the microvascular network embedded in the 2D design problem shown in Fig. 3. Here, we do not incorporate the fluid temperature constraint ψ_2 in the optimization process because it significantly confines the search space and results in very similar network configurations. Instead, by removing this constraint, we obtain a better insight into the optimized configurations of the embedded network and possible patterns that can be implemented in the next attempts.

The template network implemented to evaluate the optimized network configurations is outlined on a 100×10 grid. This corresponds to $N_e = 1890$ microchannels and hence 2^{1890} possible network configurations. We first investigate the optimized configurations assuming a constant mass flow rate of $\dot{m} = 9.333$ g/min in the microvascular network. The GA optimization is initialized with a random population of $N_{\mathcal{P}} = 600$ individuals and evolved for 120,000 generations. The pareto-optimized front for this problem and its projection on the principal planes of the Cartesian coordinate system are illustrated in Fig. 4. The best individuals

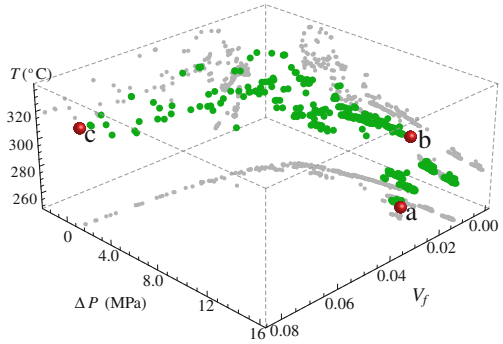

Fig. 4 Pareto-optimized front after 120,000 generations for the full-domain optimization with the constant flow rate design strategy. Each axis corresponds to one of the objective functions and the lighter nodes indicate the projection of the optimized front on the principal planes of the coordinate system. The three individuals marked as (**a**–**c**) represent the best solutions with respect to each objective function and are presented in Fig. 5

with respect to each objective function are marked in this figure and their configuration and the corresponding temperature fields in the microvascular material are presented in Fig. 5.

The competing nature of the objective functions used to determine the optimized network configurations is evident in Fig. 4. For instance, the best individual with respect to the pressure drop, shown in Fig. 5c, is among the worst with respect to the other two objective functions. The maximum temperature of the microvascular plate with the embedded network corresponding to this individual is $T_{\max} = 312.5\ ^\circ\text{C}$, which is even higher than that of the no-flow condition. This is due to the inappropriate configuration of the network, where the coolant flows in the hot region along the top edge for too long, without exchanging the heat with the colder region near the bottom edge. As the fluid approaches the right side of the domain, it eventually becomes warmer than the surrounding material and increases the temperature in that region. As another example, the network with the lowest corresponding void volume fraction, depicted in Fig. 5b, collects all the flow in one single microchannel between the inflow and the outflow vertices. However, this configuration can not properly redistribute the heat in the domain and thus efficiently contribute to cooling of the plate. Because the primary objective is to reduce the maximum temperature of the system, these two networks and other similar configurations are not appropriate candidates for the final design pattern.

The best network configuration for minimizing the maximum temperature in the microvascular plate is depicted in Fig. 5a. As discussed earlier, proper network configurations for active cooling of large domains must effectively redistribute the heat within the domain and provide efficient heat exchange between the colder and warmer regions of the material. As shown in Fig. 5a, most of the fluid is collected in a single path to increase the flow rate and hence the heat convection in the microchannel. The oscillations of the resulting network between the top and the bottom edges of the domain enables the coolant to transfer the heat from the hot region to the colder area and reduce the maximum temperature to $T_{\max} = 257.6\ ^\circ\text{C}$.

The Pareto-optimized front for the constant power design strategy and the associated temperature fields for the individuals that minimize each objective function are shown in Figs. 6 and 7, respectively. The reference power adopted here is $P = 74.86$ W, which is equal to the average power required for pumping the coolant through the networks on the Pareto-optimized front obtained from the constant flow rate design strategy, shown in Fig. 4. Comparing Figs. 4 and 6 indicates that the upper bound of the pressure drop for the optimized front associated with the constant power strategy is considerably smaller than that of the constant flow rate case. This is due to the adjustment of the mass flow rate for the constant power design based on the configuration of the network, which according to (7), directly affects the pressure drop in the microchannels.

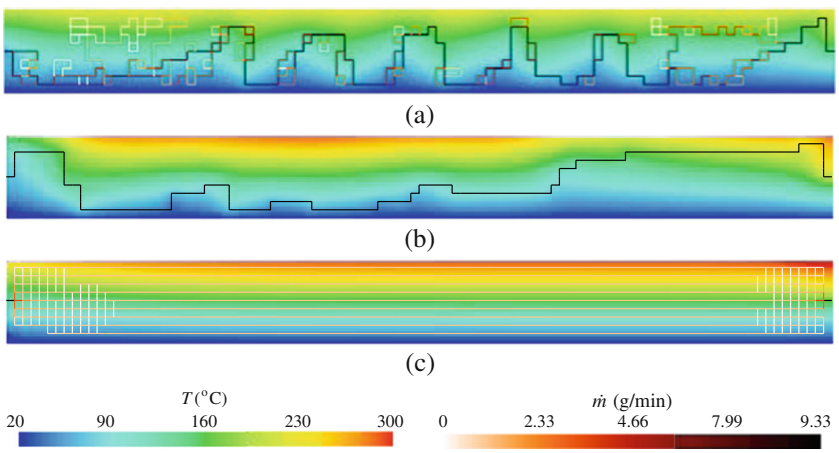

Fig. 5 Full-domain GA optimization with the constant flow rate strategy. Best configurations for minimizing **a** the maximum temperature of the material, **b** the void volume fraction, and **c** the pressure drop, corresponding to the individuals labeled as a, b, and c in Fig. 4, respectively. The *color bars* show the temperature distribution in the microvascular plate and the mass flow rate in the microchannels

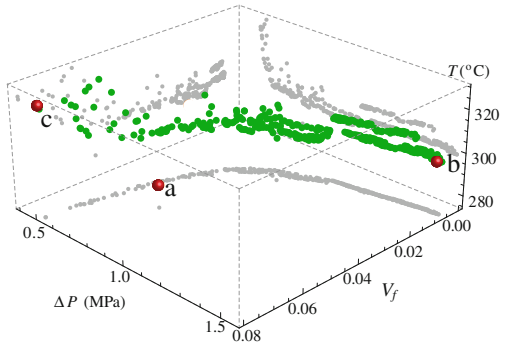

Fig. 6 Pareto-optimized front after 120,000 generations for the full-domain optimization with the constant power design strategy. The three individuals marked as (**a**–**c**) represent the best solutions with respect to each objective function and are presented in Fig. 7

The best solutions with respect to the void volume fraction and the pressure drop are shown in Fig. 7b and c, respectively. The network configuration for these individuals are very similar to the corresponding optimized solutions for the constant flow rate design strategy depicted in Fig. 5b and c. However, the configuration of the network that minimizes the maximum temperature of the plate, depicted in Fig. 7a, is very different than that with the constant flow rate strategy shown in Fig. 5a. Unlike the latter case, where the flow is mostly collected in a single path, the constant power strategy leads to a configuration that branches out to reduce the pressure drop and thus receive a higher flow rate. This tradeoff between the pressure drop and the mass flow rate, however, does not yield an appropriate configuration for reducing the maximum temperature of the plate. The reasons are twofold: (i) this network configuration cannot effectively redistribute the heat within the plate and (ii) the low velocity of the coolant due to dividing the inflow between multiple microchannels weakens the associated heat convection. Note that the maximum temperature of the microvascular material in this case is $T_{\max} = 285.7\,^{\circ}\mathrm{C}$, which is considerably higher than $T_{\max} = 257.6\,^{\circ}\mathrm{C}$ obtained for the constant flow rate design. Moreover, although the pressure drop associated with the network depicted in Fig. 7a is significantly lower than that of the constant flow rate strategy, the void volume fraction in the latter case is considerably higher.

6 GA optimization: periodic boundary conditions

The full-domain GA optimization results presented in the previous section are obtained via computationally demanding simulations, which is one of the main disadvantages of this approach. Another major drawback is the complex configurations of the optimized networks, which are often not suitable for manufacturing purposes. Moreover, the presence of isolated individuals on the optimized fronts (especially the individual labeled a in Fig. 6) indicates that there is more room for improvement in the resulting optimized configurations. Therefore, more optimized configurations has not shown up in the results of these simulations. Nevertheless, the results presented in the previous section provide a good insight on the optimal network configurations. It must be noted that better configurations could be obtained by increasing the size of the initial population, but it would increase the computational cost even further.

In this section, we introduce a new optimization problem by using the information obtained from Fig. 5a as *a priori* knowledge regarding the optimized configuration of the network. That network configuration minimizes the maximum temperature of the microvascular plate for the constant flow rate design strategy. Inspired by this result, we aim to find optimized designs with the extra constraint of periodic configurations. As shown in Fig. 5a, a similar pattern is observable, where the network oscillations are repeated along the length of the domain. It must be noted that, the periodic configuration suggested by the GA results for the embedded network in this problem is similar to the

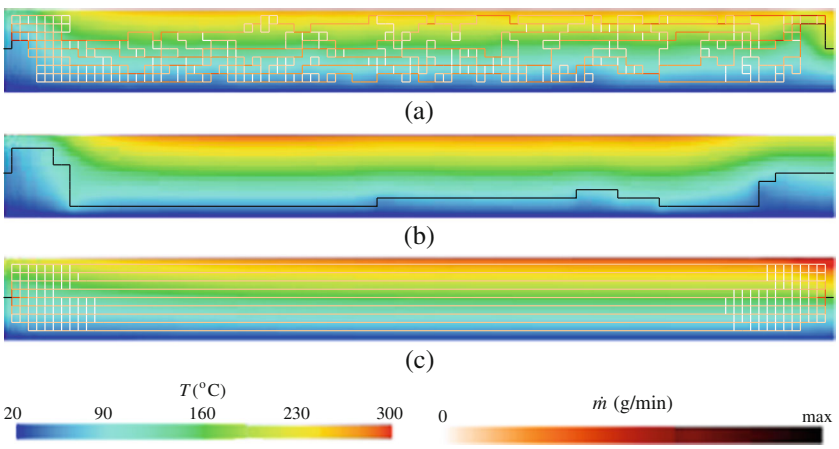

Fig. 7 Full-domain GA optimization with the constant power strategy. Best configurations for minimizing **a** the maximum temperature of the material, **b** the void volume fraction, and **c** the pressure drop, corresponding to the individuals labeled as a, b, and c in Fig. 6, respectively

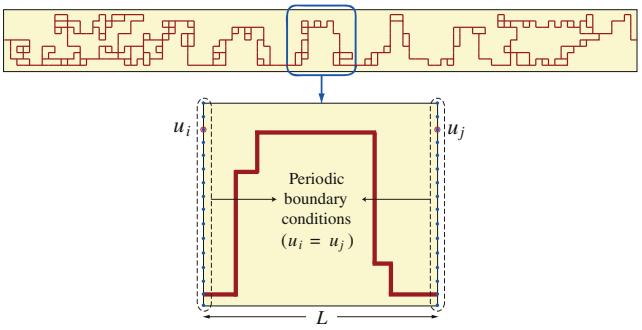

Fig. 8 Schematic of the GA optimization with periodic boundary conditions over a small subdomain of the original problem with the length of L

microvascular blood vessels used for the thermal regulation in the human skin (Soghrati et al. 2012a). Using the assumption of period state of the temperature in the actively-cooled system, the problem of finding the optimized network configuration can then be replaced by a new optimization problem over a smaller subdomain with a length equal to the wavelength of the periodic network (Fig. 8). Because the periodic cell lengths associated with the optimized network configurations are unknown before running the simulations, we perform the optimization over several subdomains with different lengths to also incorporate the wavelength of the network as one of the design parameters. However, due to the small size of each subdomain, the number of generations needed to achieve convergence and the cost of evaluating the temperature field in them are considerably lower than those of the original problem.

Another issue that must be addressed here is the boundary conditions applied to each periodic subdomain. While the boundary conditions along the top and the bottom edges

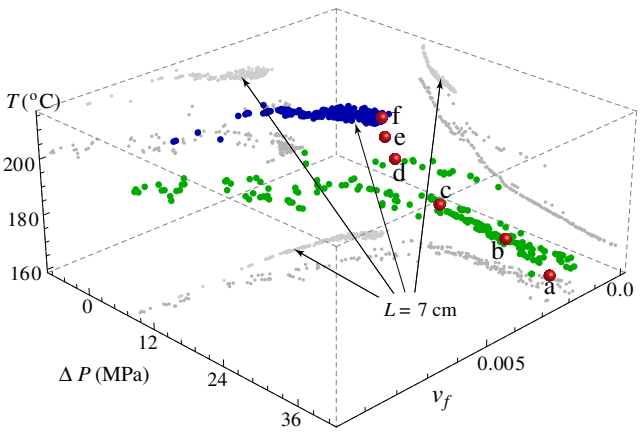

Fig. 9 Pareto-optimized fronts associated with $L = 2$ and $L = 7$ cm for the constant flow rate design strategy with periodic boundary conditions after 10,000 generations. The six individuals labeled (**a**–**f**) correspond to the the network configurations that minimize the maximum temperature of the subdomains with $L = 2$, 3, 4, 5, 6, and 7 cm, respectively

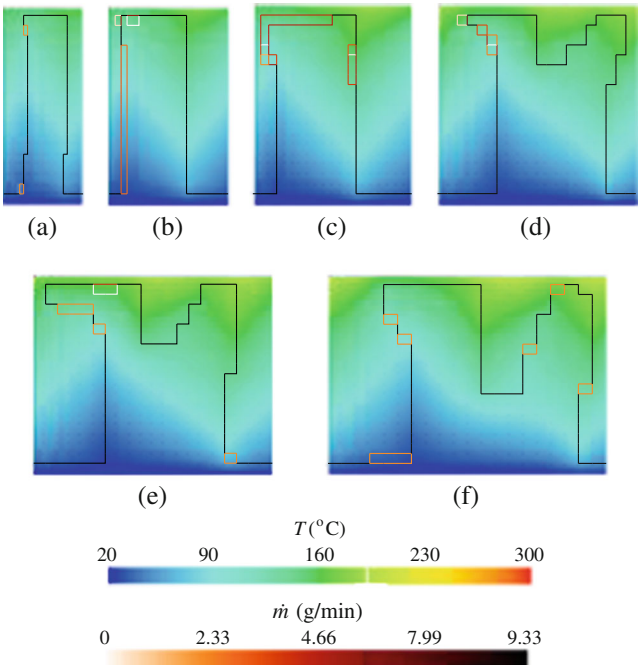

Fig. 10 Network configurations that minimize the maximum temperature of the system and the corresponding temperature fields for the GA optimization with periodic boundary conditions and the constant flow rate design strategy. The subdomains shown in (**a**–**f**) represent the individuals labeled similarly on the Pareto-optimized front, shown in Fig. 9, with $L = 2$, 3, 4, 5, 6, and 7 cm, respectively

are unchanged, those of the left and the right edges must be revised. As schematically shown in Fig. 8, the periodic boundary condition is imposed along these edges by assigning the same equation number in the discretized system to the finite element nodes with the same vertical coordinate. We also do not specify the inlet temperature of the coolant in these subdomains and use the periodic boundary

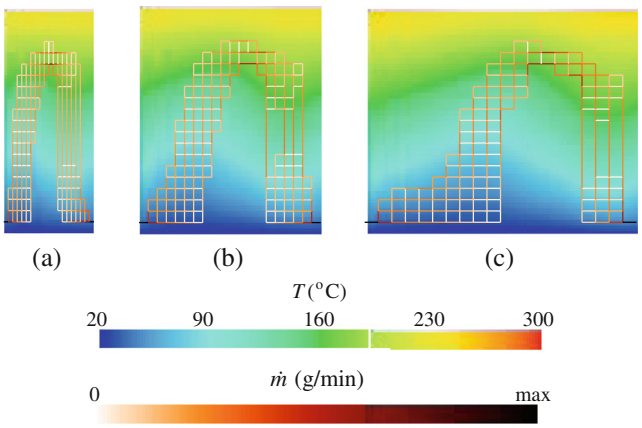

Fig. 11 Optimized network configurations that minimize the maximum temperature of the system and the associated temperature fields for the optimization with periodic boundary conditions and the constant power design strategy. The length of the subdomains depicted in (**a**–**c**) equals 2, 4, and 6 cm, respectively

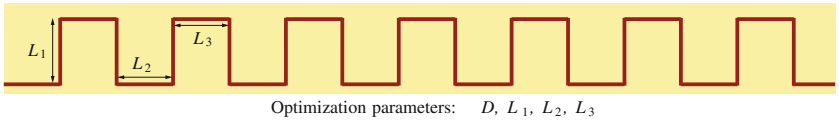

Fig. 12 Schematic of the network configuration and the associated design parameters adopted in the parametric shape optimization problem

condition at the inlet and outlet nodes, for which the coolant temperature at the inlet can be determined from FEM simulations. Note that a periodic state for the temperature field in the microvascular system appears only after the coolant passed a certain number of periodic cells. Since the fluid temperature at the entrance, $T_{\text{in}} = 20\,^{\circ}\text{C}$, is less than that of the surrounding material, the temperature of the coolant at the beginning of each periodic cell length is constantly increasing before the periodic state. Therefore, the maximum temperature of the actively-cooled microvascular plate appears in this periodic state, where the coolant temperature is at its highest.

The Pareto-optimized fronts for the constant flow rate design strategy is presented in Fig. 9. The subdomains studied in this figure have lengths ranging from 2 to 7 cm, with increments of 1 cm. For the sake of clarity, we have only shown the optimized fronts corresponding to $L = 2$ and $L = 7$ cm in Fig. 9. However, the best solutions for minimizing the maximum temperature associated with all the length scales are marked as (a–f) there. The GA population used for each subdomain has a size of $N_p = 200$, which is evolved for 10,000 generations. Moreover, the grid used to construct the template network is three times more refined than that of the full-domain optimization problem, which yields improved optimized network configurations. Note that the overall computational cost associated with this second level of optimization is less than 1 % of that of the original design optimization problem.

The network configurations that minimize the temperature of each subdomain and the corresponding temperature fields in the microvascular material are depicted in Fig. 10. The best solution for the maximum temperature objective function yields $T_{\max} = 178.8\,^{\circ}\text{C}$, which is clearly more optimized than that obtained from the original optimization problem, i.e., $T_{\max} = 285.7\,^{\circ}\text{C}$. For smaller subdomains, i.e., $L = 2$, 3, and 4 cm, the resulting networks exchange the heat between the cold and the hot regions of the domain through a single square-wave-shape microchannel. For larger subdomains, the configuration of the embedded network is affected by the periodic cell length of the network, such that more than one oscillation is observed. This is due to the efficient active cooling achieved when the coolant flowing along the top edge returns to the cold region and releases the heat before it becomes too hot and loses its cooling capacity. Thus, more than one oscillation is required for networks with larger periodic cell lengths to avoid excessive increase in the temperature of the coolant. This behavior is clearly observable in Fig. 10f, where the optimized embedded network with a periodic cell length of $L = 7$ cm shows two almost complete oscillations.

The three network configurations with periodic cell lengths 2, 4, and 6 cm that minimize the temperature of the system for the constant power design strategy are illustrated in Fig. 11. These results reveal a similar behavior as the full-domain optimization study presented in the previous section. Similar to those results, both the maximum temperature and the void volume fraction of the microvascular material are considerably higher than those of the corresponding subdomains designed with the constant flow rate strategy, shown in Fig. 10. For the current case, the network divides into multiple branches to reduce the pressure drop and receive a higher flow rate from the constant source of power. However, the underlying mechanism for active

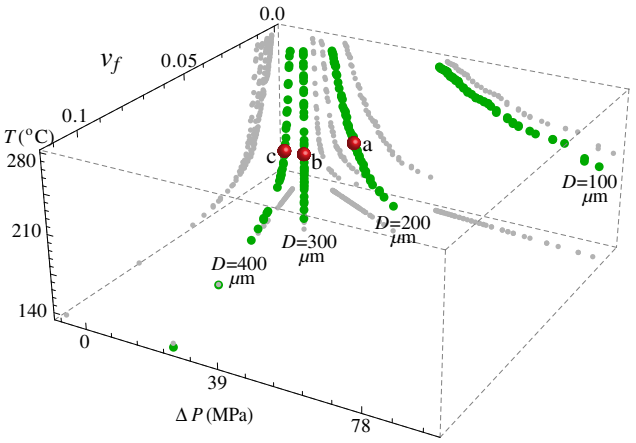

(a)

Optimization parameter	Number of choices	Minimum value (mm)	Maximum value (mm)	Increments (mm)
D	4	0.1	0.4	0.1
L_1	8	5	40	5
L_2	16	5	80	5
L_3	16	5	80	5

(b)

Fig. 13 **a** Pareto-optimized front for the parametric shape optimization problem with the population $N_P = 200$. The individuals marked as a, b, and c correspond to the networks that yield $T_{\max} \approx 200\,^{\circ}\text{C}$ with $D = 200$, 300, and 400 μm, respectively, as shown in Fig. 14. **b** Range of the design parameters used to obtain the optimized front

cooling of the material is similar to that of the constant flow rate strategy. Here too, the network oscillations along the top and the bottom edges, i.e., the hot and the cold regions, contribute to redistributing the heat within the material and reducing its temperature.

7 Shape optimization study

As discussed in the previous section, the network that minimizes the temperature of the system for the constant flow rate design strategy can be modeled as a single orthogonal-wave-shape microchannel. Inspired by that study, we adopt this geometric shape as the final configuration of the embedded network, as shown in Fig. 12. The optimization problem is then reduced to evaluating the optimal values of the microchannel diameters D and the lengths L_1, L_2, and L_3, to satisfy the fluid temperature constraint and minimize the three objective functions introduced earlier. We use a constant flow rate design strategy for each diameter, where similar to the previous sections, $\dot{m} = 9.33$ g/min for $D = 200$ μm. For other diameters, $\dot{m}$ is adjusted proportionally to maintain a constant Reynolds number in the microchannels. Therefore, the microchannels with larger diameters collect a higher flow rate and more effectively reduce the material's temperature. Note that, despite a higher flow rate, the pressure drop associated with larger diameters is reduced considerably due to the D^{-4} relationship between the pressure drop and the diameter as given in (7).

The advantages of the proposed shape optimization scheme compared to the GA optimization problems studied in the previous sections are twofold. The first advantage is reducing the complexity of the network configuration to better suit the manufacturing constraints. Moreover, constraints such as the minimum and the maximum values of the wavelength of the network can be easily incorporated in this parameter study. The second advantage is the extremely low computational cost of the current study compared to the previous GA simulations. In this case, the size of the search space is usually small enough to evaluate the objective functions for all possible network configurations. We then select a few individuals as the optimized front using the non-dominated sorting algorithm implemented in the NSGA-II (Deb et al. 2002). The computational cost associated with these simulations is approximately 2 % of the GA optimization with the periodic boundary conditions studied in the previous section.

The optimized front for the current shape optimization study and the values of the parameters used to describe the microchannel configurations are presented in Fig. 13. As shown in Fig. 13a, the optimized front is composed of 200 individuals (among 4096 possible configurations), where each cluster on this plot represents individuals associated with one of the microchannel diameters. As expected, embedded microchannels with larger diameters are more effective in reducing the maximum temperature and yield a lower pressure drop. However, this leads to a microvascular material with a higher void volume fraction and hence may deteriorate its structural stiffness. Note that compared to $T_{\max} = 178.8\,^{\circ}$C as the lowest maximum temperature for the periodic boundary condition problem, the best individual for minimizing the maximum temperature of the system with $D = 200$ mm yields $T_{\max} = 158.9\,^{\circ}$C.

As a final note, we use the optimized front depicted in Fig. 13a to design the embedded microchannel for an allowable temperature of $T_{\text{all}} = 200\,^{\circ}$C in the actively-cooled epoxy plate. Figure 14 illustrates the microchannel configurations and the corresponding temperature fields in the material for the three individuals labeled in Fig. 13a. Because the maximum temperature is approximately identical for these three networks, i.e., $T_{\max} \approx 200\,^{\circ}$C, the other two objective functions determine the optimized microchannel configuration. First, note that none of the network configurations with $D = 100\,\mu$m are able to reduce

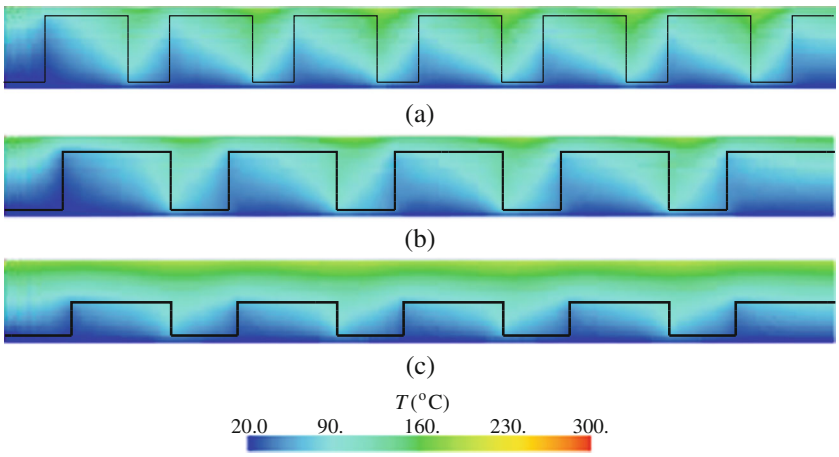

Fig. 14 Network configurations and corresponding temperature field for the three individuals labeled similarly in Fig. 13a

the maximum temperature to a value less than 210 °C. Thus, we can not use this diameter to design a microvascular material with $T_{all} = 200$ °C. Among the microvascular systems presented in Fig. 14, the lowest void volume fraction and the highest pressure drop are associated with the microchannel with $D = 200\,\mu$m (Fig. 14a). This configuration is thus the appropriate choice if the potential impact on the structural stiffness of the material is more important than the flow efficiency. However, if the main objective is to minimize the required power and the importance of the stiffness comes second, the network with $D = 400\,\mu$m as shown in Fig. 14c is the best choice.

8 Conclusion

The design of the network embedded in an actively-cooled microvascular epoxy plate was presented using a three-step GA-inspired FEM-based approach. Designing the network was initiated by defining an optimization problem over the entire domain of the microvascular material. We employed the NSGA-II to determine the optimized network configurations that minimize the maximum temperature, the void volume fraction associated with the embedded microchannels, and the pressure drop needed to circulate the coolant. Although this study was computationally demanding and the resulting optimized networks were often too complex to manufacture, it provided insight on the candidate optimized designs of the actively-cooled material. Based on that study, we adopted a periodic configuration for the microvascular network. The original problem was then replaced by several smaller problems, for which the computational cost and the complexity of the optimized networks were considerably lower. That study suggested that an square-wave-shape microchnnel yields the most efficient active cooling in the system. Therefore, we performed a parametric shape optimization to determine the optimized values of the wavelength, amplitude, and the diameter of the square-wave-shape microchannel. Those results were obtained at a small fraction of the computational cost of the former GA optimization studies. Throughout this work, we also studied two different design strategies: a constant power and a constant inflow rate. We observed that the former leads to considerably less efficient designs for reducing the maximum temperature of the system. Moreover, we showed that the square wave configuration is the optimized design for both strategies, but tends to divide into more branches if the constant power strategy is adopted.

Acknowledgments This work has been supported by the Air Force Office of Scientific Research Multidisciplinary University Research Initiative (Grant No. FA9550-09-1-0686). The authors wish to acknowledge insightful discussions with Prof. S. R. White and Prof. N. R. Sottos at the University of Illinois.

References

Aragón AM, Wayer JK, Geubelle PH, Goldberg DE, White SR (2008) Design of microvascular flow networks using multi-objective genetic algorithms. Comput Methods Appl Mech Eng 197:4399–4410

Aragón AM, Smith KJ, Geubelle PH, White SR (2011) Multi-physics design of microvascular materials for active cooling applications. J Comput Phys 230(13):5178–5198

Bejan A (1997) Constructal-theory network of conducting paths for cooling a heat generating volume. Int J Heat Mass Transfer 40(4):799–816

Bejan A, Lorente S (2008) Design with constructal theory. Wiley, Hoboken

Brebbia CA, Ferrante A (1983) Computational hydraulics. Butterworths, London

Bronzino JD (ed) (2000) The biomedical engineering handbook, 2nd edn. CRC Press LLC, Boca Raton

Chen Y, Zhou S, Li Q (2010) Multiobjective topology optimization for finite periodic structures. Comput Struct 88:806–811

Deb K, Agrawal S, Pratap A, Meyarivan T (2002) A fast and elitist multi-objective genetic algorithm: NSGA-II. IEEE Trans Evol Comput 6(2):181–197

Esser-Kahn AP, Thakre PR, Dong H, Patrick J, Sottos NR, Moore JS, White SR (2011) Three dimensional microvascular fiber-reinforced composites. Adv Mater 23(32):3654–3658

Evgrafov A (2006) Simultaneous optimization of topology and geometry of flow networks. Struct Multidiscipl Optim 32(2):99–109

Fonseca CM, Fleming PJ (1993) Genetic algorithms for multiobjective optimization: formulation, discussion and generalization. In: Forrest, S (ed) Genetic algorithms: proceedings of the fifth international conference, pp 416–423

Gersborg-Hansen A, Sigmund O, Haber RB (2005) Topology optimization of channel flow problems. Struct Multidiscipl Optim 30(3):181–192

Goldberg DE (1989) Genetic algorithms in search, optimization, and machine learning. Addison-Wesley Publishing Company, Massachusetts

Goldberg DE (2002) The design of innovation: lessons from and for competent genetic algorithms. Kluwer Academic Publishers, Massachusetts

Hansen CJ, Wu W, Toohey KS, Sottos NR, White SR, Lewis JA (2009) Self-healing materials with interpenetrating microvascular networks. Adv Mater 21(41):4143–4147

Horn J, Nafpliotis N, Goldberg DE (1994) A niched pareto genetic algorithm for multiobjective optimization. In: IEEE world congress on computational intelligence. Proceedings of the first IEEE conference on evolutionary computation, vol 1, pp 82–87

Kays WM, Crawford ME, Weigand B (2004) Convective heat and mass transfer, 4th edn. McGraw-Hill, New York

Klarbring A, Petersson J, Torstenfelt B, Karlsson M (2003) Topology optimization of flow networks. Comput Methods Appl Mech Eng 192(35-6):3909–3932

Kozola BD, Shipton LA, Natrajan VK, Christensen KT, White SR (2010) Characterization of active cooling and flow distribution in microvascular polymers. J Intell Mater Syst Struct 21(12):1147–1156

Kukkonen S, Lampinen J (2005) GDE3: the third evolution step of generalized differential evolution. In: The 2005 IEEE congress on evolutionary computation, vol 1, pp 443–450

Kumar SV, Doby TA, Baugh JW Jr, Brill ED, Ranjithan SR (2006) Optimal design of redundant water distribution networks using a cluster of workstations. J Water Resour Plan Manag 132(5):374–384

Nible E, Pinto F, Rizzetto G (2006) Geometric parameterization and multiobjective shape optimization of convective periodic channels. Numer Heat Transf B Fundam Int J Comput Methodol 50:425–453

Olugebefola SC, Aragón AM, Hansen CJ, Hamilton AR, Kozola BD, Wu W, Geubelle PH, Lewis JA, Sottos NR, White SR (2010) Polymer microvascular network composite. J Compos Mater 44(22):2587–2603

Oueslati RB, Therriault D, Martel S (2008) PCB-integrated heat exchanger for cooling electronics using microchannels fabricated with the direct-write method. IEEE Trans Components Packag Technol 31(4):869–874

Park K, Choi DH, Lee KS (2004) Optimum design of plate heat exchanger with staggered pin arrays. Numer Heat Transfer A Appl Int J Comput Methodol 45:347–361

Pastukhov VG, Maidanik YF, Vershinin CV, Korukov MA (2003) Miniature loop heat pipes for electronics cooling. Appl Therm Eng 23(9):1125–1135

Prasad TD, Park N (2004) Multiobjective genetic algorithms for design of water distribution networks. J Water Resour Plan Manag 130(1):73–82

Rozavany GIN (2009) A critical review of established methods of structural topology optimization. Struct Multidicipl Optim 37:217–237

Shipton LA (2007) Thermal management applications for microvascular systems. Master's thesis. University of Illinois at Urbana-Champaign

Sigmund O (2011) On the usefulness of non-gradient approaches in topology optimization. Struct Multidiscipl Optim 43(5):589–596

Simpson AR, Dandy GC, Murphy LJ (1994) Genetic algorithms compared to other techniques for pipe optimization. J Water Resour Plan Manag 120(4):423–443

Soghrati S, Geubelle PH (2012) A 3D interface-enriched generalized finite element method for weakly discontinuous problems with complex internal geometries. Comput Methods Appl Mech Eng 217-220:46–57

Soghrati S, Thakre PR, White SR, Sottos NR, Geubelle PH (2012a) Computational modeling and design of actively-cooled microvascular materials. Int J Heat Mass Transf 55:5309–5321

Soghrati S, Aragón AM, Duarte CA, Geubelle PH (2012b) An interface-enriched generalized finite element method for problems with discontinuous gradient fields. Int J Numer Methods Eng 89(8):991–1008

Toohey KS, Sottos NR, Lewis JA, Moore JS, White SR (2007) Self-healing materials with microvascular networks. Nat Mater 6:581–585

Wang Y, Yuan G, Yoon YK, Allen MG, Bidstrup SA (2005) Active cooling substrates for thermal management of microelectronics. IEEE Trans Components Packag Technol 28(3):477–483

Wei X, Joshi Y, Patterson MK (2007) Experimental and numerical study of a stacked microchannel heat sink for liquid cooling of microelectronic devices. J Heat Tran 129(10):1432–1444